

Energy Efficiency and Reliability in Wireless Biomedical Implant Systems

Jamshid Abouei, *Member, IEEE*, J. David Brown, Konstantinos N. Plataniotis, *Senior Member, IEEE* and Subbarayan Pasupathy, *Life Fellow, IEEE*

Abstract—The use of wireless implant technology requires correct delivery of the vital physiological signs of the patient along with the energy management in power-constrained devices. Toward these goals, we present an augmentation protocol for the physical layer of the Medical Implant Communications Service (MICS) with focus on the energy efficiency of deployed devices over the MICS frequency band. The present protocol uses the rateless code with the Frequency Shift Keying (FSK) modulation scheme to overcome the reliability and power cost concerns in tiny implantable sensors due to the considerable attenuation of propagated signals across the human body. In addition, the protocol allows a fast start-up time for the transceiver circuitry. The main advantage of using rateless codes is to provide an inherent adaptive duty-cycling for power management, due to the flexibility of the rateless code rate. Analytical results demonstrate that an 80% energy saving is achievable with the proposed protocol when compared to the IEEE 802.15.4 physical layer standard with the same structure used for wireless sensor networks. Numerical results show that the optimized rateless coded FSK is more energy efficient than that of the uncoded FSK scheme for deep tissue (e.g., digestive endoscopy) applications, where the optimization is performed over modulation and coding parameters.

Index Terms—Energy efficiency, green modulation, medical implants, wireless body area networks (WBANs)

I. INTRODUCTION

A. Background

Recent advances in wireless sensor technologies have opened up a new generation of ubiquitous body-centric systems, namely Wireless Body Area Networks (WBANs), for providing efficient health care services [1]. WBANs support a broad range of medical/non-medical applications in home/health care, medicine, sports, etc. Of interest is the use of WBANs for the continuous remote monitoring of the vital physiological signs of patients, regardless of the constraints on their locations and activities [2].

Broadly, WBANs can be classified into two categories of wearable (on-body) and implantable (in-body) systems [3],

Manuscript received November 28, 2010; accepted January 4, 2011. The work was supported in part by an Ontario Research Fund (ORF) project entitled “Self-Powered Sensor Networks”. The work of J. Abouei was performed when he was with the Department of Electrical and Computer Engineering, University of Toronto, Toronto, ON M5S 3G4, Canada.

J. Abouei is with the Department of Electrical and Computer Engineering, Yazd University, Yazd, Iran (e-mail: abouei@yazduni.ac.ir).

J. D. Brown is with the DRDC Ottawa, Ottawa, ON, Canada. He completed his Ph.D. in ECE at University of Toronto (e-mail: david_jw_brown@yahoo.com).

K. N. Plataniotis, and S. Pasupathy are with the Edward S. Rogers Sr. Department of Electrical and Computer Engineering, University of Toronto, Toronto, ON M5S 3G4, Canada (e-mails: {kostas, pas}@comm.utoronto.ca).

TABLE I
COMPARING SOME MICS SPECIFICATIONS WITH THE IEEE 802.15.4 STANDARD USED FOR WSNs

Parameter	MICS	IEEE 802.15.4
Frequency Band	402 – 405 MHz	868/915 MHz (Eur./US) 2.4 GHz (Worldwide)
Bandwidth	300 KHz	62.5 KHz (for 2.4 GHz)
Data Rate	support more than 250 kbps	250 kbps (for 2.4 GHz)
Transmit Power	25 μ w (–16 dBm)	0.5 mw (–3 dBm)
Operating Range	Typically 0 – 2 m	Typically 0 – 10 m

[4]. A wearable WBAN provides RF communications between on-body sensors and a central controller for the remote monitoring of vital signs of a patient such as ECG, blood pressure and temperature. Such a wearable structure is a short-range communication system based on the Wireless Medical Telemetry Service (WMTS) officially adopted by the Federal Communications Commission (FCC) [5]. On the other hand, in an implantable WBAN, a biosensor embedded within the body communicates with an apparatus sticking on the body or with an external monitoring device in the vicinity of the human body. Examples of implantable devices are cardiac pacemakers, insulin dispensers, neurostimulators and bladder controllers [6]. Such a wireless implantable technology is a very short-range communication system used for monitoring health conditions of patients such as brain waves in paralyzed persons, glucose levels in diabetic patients and patients with gastrointestinal disorders. The medical implantable devices operate according to the Medical Implant Communications Service (MICS) rules established by FCC [7].

The MICS standard is distinguished from the existing standards used for Wireless Sensor Networks (WSNs) [8], [9] due to the size, power consumption and frequency band requirements for implantable devices (see Table I). For instance, the MICS protocol uses an 25 μ W (–16 dBm) Effective Isotropic Radiated Power (EIRP) at the 402–405 MHz frequency band. This provides a low power transmitter with a small size antenna resulting in a compact and lightweight implantable device, while, today’s low power radio devices which use standards such as ZigBee and Bluetooth (IEEE 802.15.1) cannot meet these stringent requirements. Furthermore, the limit –16 dBm EIRP in the MICS standard reduces the effect of the interference on the other biosensor devices operating in the same frequency band [7]. In addition, deploying ultra low power devices minimizes the heat absorption and the temperature increase caused by implantable biosensors, reducing the thermal effects on the body tissues [10].

Besides the simplicity and low power consumption characteristics, implantable devices must be robust enough to provide the desired service for long-term applications. Furthermore, since biosensors frequently switch between the sleep mode and the active mode, they should have fast start-up times. The protocol used for such implantable devices must support a high degree of reliability and energy efficiency in a realistic channel model for the human body. Each of these characteristics presents considerable design challenges for different layers of implantable WBANs, including the MAC layer and the physical layer [11]–[13]. Central to the study of the physical layer design of implantable WBANs is the modulation and coding. Deploying proper modulation schemes which minimize the total energy consumption in both circuit and RF signal transmission prolongs the biosensors lifetime. Enhanced reliability, on the other hand, is achieved by adding redundant information bits in the data packets in the Forward Error Correction (FEC) coding stage at the cost of an extra power consumption. Thus, there is generally a trade-off between a higher reliability and a lower power consumption in using FEC codes.

B. Related Work and Contribution

There are several works in the literature that study the physical layer design of implantable WBANs. Oh *et al.* [11] propose a new type of phase shift keying modulation scheme, namely Phase Silence Shift Keying (PSSK), for high data rate implantable medical devices which is more bandwidth efficient than orthogonal modulation schemes such as OOK. Under an Additive White Gaussian Noise (AWGN) channel model with path loss for the human body, reference [11] shows that the Bit Error Rate (BER) of an 8-PSSK is lower than that of various sinusoidal carrier-based modulation schemes. Reference [12] proposes a simple and ultra low power hardware design for an FSK/MSK direct modulation transmitter in medical implant communications which supports the data rate and the EIRP requirements in the MICS standard. However, no channel coding scheme and energy efficiency analysis were considered in [11] and [12]. Reference [14] investigates the feasibility of applying an Ultra-Wideband (UWB) scheme to implantable applications. However, according to the FCC regulations in [15], UWB technologies with a typically 3–10 GHz frequency band are used for transmitting information over a wide bandwidth at least 500 MHz, which are wider than the frequency band and the bandwidth used in the MICS standard.

Since, the human body is a lossy medium, and due to the adverse circumstances in the patient's body (e.g., variable body temperature due to the fever, changing the location of the implant capsule in the digestive system), the RF signal transmitted from the in-body biosensor experiences a dynamic channel environment to reach to its corresponding on-body receiver. In addition, it is shown in [16] that the efficiency of wireless implantable devices is related to the human body structure (e.g., male or female, body size, obese or thin and tissue composition). Clearly, finding a proper FEC coding scheme which overcomes the patient's vital information loss, and operates in a high degree of flexibility and accuracy over

the above dynamic channel conditions is desirable. Existing protocols use various methods to overcome the packet loss and decoding error concerns in classical wireless sensor networks (e.g., see [17]). The Automatic Repeat Request (ARQ) approach, for instance, requires many retransmissions in the case of poor channel conditions, resulting in a high latency in the network. This is in contrast to the transmission of patient's real time vital signs which are sensitive to the latency. More recently, the attention of researchers has been directed toward deploying rateless codes (e.g., Luby Transform (LT) code [18]) in conventional wireless networks due to the significant advantages of these codes in erasure channels. However, to the best of our knowledge, there is no existing analysis on the energy efficiency and reliability of rateless coded modulation in implant WBANs.

This work deals with the first in-depth analysis on the energy efficiency and reliability of a wireless biomedical implant system which uses LT codes with the Frequency Shift Keying (FSK) modulation scheme. The present analysis is based on a realistic channel model for the human body as well as the requirements stated in the MICS standard. The main outcome of this work is to introduce an augmentation protocol for the physical layer of the MICS standard for implant WBANs. The protocol allows a fast start-up time for implantable devices along with the lower power consumption during active mode duration. It is demonstrated that an 80% energy saving is achievable compared to the IEEE 802.15.4 physical layer protocol with the same structure used for wireless sensor networks. Furthermore, we show that an inherent adaptive duty-cycling for power management is provided which comes from the flexibility of the LT code rate. Numerical results for deep tissue applications show a lower energy consumption in the optimized coded scheme compared to the uncoded case.

The rest of the paper is organized as follows. In Sections II and III, the implant wireless system based on a realistic channel model for the human body is described. The energy consumption of an uncoded FSK modulation scheme is analyzed in Section IV. Design of LT codes and the energy efficiency of the LT coded FSK are presented in Section V. Section VI provides some numerical evaluations using realistic parameters to confirm our analysis. Also, some design guidelines for using LT codes in practical implant WBANs are presented. Finally in Section VII, an overview of the results and conclusions are presented.

II. SYSTEM MODEL AND ASSUMPTIONS

In this work, we consider a wireless biomedical implant system depicted in Fig. 1 with a bidirectional communication between an implantable biosensor, denoted by IBS, and an external Central Control Unit (CCU), where the transmission in each direction takes place in a half-duplex mode. We define the link used for the transmission of signals from the IBS to the CCU as an *uplink*, while the link from the CCU to the IBS is represented as a *downlink*. During the uplink transmission period, the IBS wakes up after receiving a command signal from the CCU, and transmits the processed raw physiological signals to the CCU. For this period, the CCU is set to the

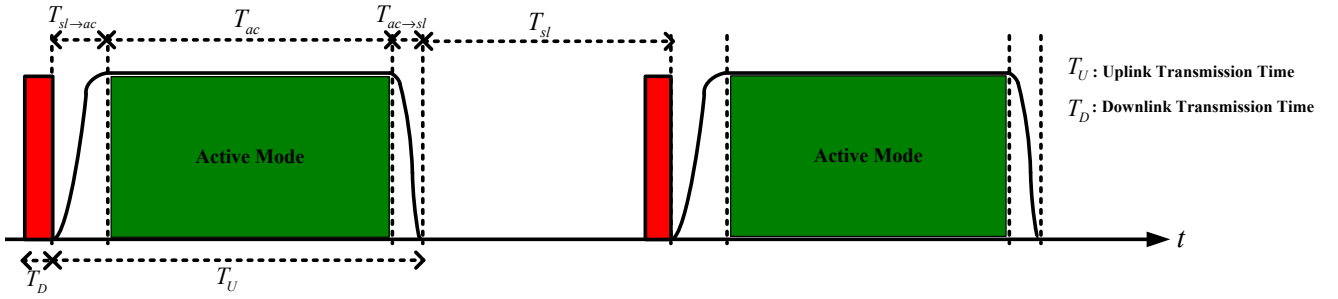


Fig. 2. A practical multi-mode operation in a reactive implant WBAN.

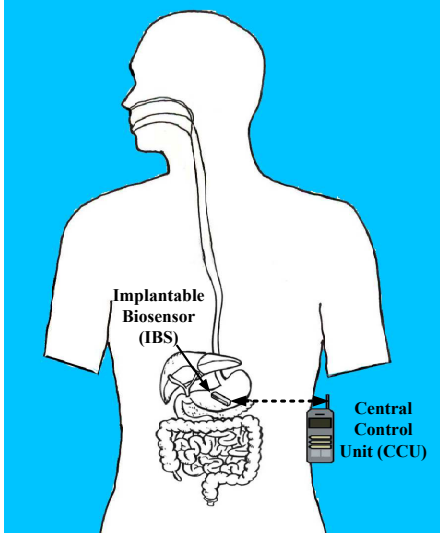


Fig. 1. A wireless biomedical implant system.

listen mode. For the downlink transmission interval, the IBS is switched to the listen mode to receive control commands from the CCU. It is worth mentioning that uplink has much more data to transmit than downlink, meaning the downlink transmission time is much smaller than that of the uplink. The main advantage of this half-duplex operation is that a common carrier is shared between the uplink and the downlink (by switching the bandwidth resource in time), resulting in further reduction of the IBS complexity. In addition, in contrast to the full-duplex systems, where they use two different frequency bands for transmitting and receiving signals, using the half-duplex solution maximizes the data rate for each link over the whole bandwidth. This arises from the Shannon capacity formula $C = B \log_2(1 + \text{SNR})$, where the channel capacity C is proportional to the bandwidth B . The assumption of half-duplex operation is used in many studies on this topic (e.g., see [16] for implant WBANs). Longer transmission time for the uplink compared to the downlink time interval makes the uplink to be considered as a critical path in wireless in-body communications from the power consumption point of view. More precisely, unlike the CCU which has a power source, the IBS has power constraint, and it needs to reduce its power consumption for minimizing the tissue heating, extending the battery life in the IBS and meeting the power restriction in the MICS standard. For this purpose, we introduce a synchronized

switching process which achieves a significant energy saving in the uplink mode.

For the proposed communication system, the IBS and the CCU must synchronize with one another and operate in a real time based process known as *duty-cycling* as depicted in Fig 2. During the *active mode* period T_{ac} for the uplink data path, the weak raw signal sensed by the implantable biosensor is first passed through the amplification and filtering processes to increase the signal strength and to remove unwanted signals and noise. The filtered analog signal is then digitized by an Analog-to-Digital Converter (ADC), and an L -bit binary message sequence $\mathbb{M}_L = \{m_i\}_{i=1}^L$ is generated, where L is assumed to be fixed. The bit stream is then sent to the FEC coding unit. The encoding process begins by dividing the message \mathbb{M}_L into blocks of equal length denoted by $\mathbb{B}_j = (m_{(j-1)k+1}, \dots, m_{jk})$, $j = 1, \dots, \frac{L}{k}$, where k is the length of any particular \mathbb{B}_j . Each block \mathbb{B}_j is encoded by a rateless code (in a manner to be described in Section V) to generate a coded bit stream $\mathbb{C}_j = (a_{(j-1)n+1}, \dots, a_{jn})$, $j = 1, \dots, \frac{L}{k}$, with block length n , where n is a random variable and is determined based on the channel condition.

The coded stream is then modulated by an FSK modulation scheme and transmitted to the CCU across tissues in the human body. We will explain later the advantages of using FSK modulation scheme in the proposed implant system. Finally, the IBS returns to the *sleep mode*, and all the circuits of the transceiver are powered off for the sleep mode duration T_{sl} for energy saving. It should be noted that only the wake-up circuit in the IBS remains on during T_{sl} , and waits for a wake-up command from the CCU. Since the wake-up circuit is battery-free (similar to that used in passive Radio Frequency Identification (RFID) tag technologies), its power consumption is very low [19]. We denote T_{tr} as the *transient mode* duration consisting of the switching time from sleep mode to active mode (i.e., $T_{sl \rightarrow ac}$) plus the switching time from active mode to sleep mode (i.e., $T_{ac \rightarrow sl}$), where $T_{ac \rightarrow sl}$ is short enough compared to $T_{sl \rightarrow ac}$ to be negligible. Furthermore, the amount of power consumed for starting up the IBS is more than the power consumption during $T_{ac \rightarrow sl}$. Under the above considerations, the IBS/CCU devices have to process one entire L -bit message \mathbb{M}_L during $0 \leq T_{ac} \leq T_L - T_{sl} - T_{tr}$ in the uplink mode before a new sensed packet arrives, where $T_L = T_{tr} + T_{ac} + T_{sl}$ with $T_{tr} \approx T_{sl \rightarrow ac}$.

Since an implant WBAN communicates over a very short-range across the human body, the circuit power consumption is

comparable to the RF transmit power consumption. We denote the total circuit power consumption in the uplink path as $P_c = P_{ct} + P_{cr}$, where P_{ct} and P_{cr} represent the power consumption of the circuits embedded in the IBS (as the transmitter) and the CCU (as the receiver), respectively. In addition, the power consumption of RF signal transmission in the IBS is denoted by P_t . Taking these into account, the total energy consumption during the active mode period in uplink, denoted by E_{ac} , is given by $E_{ac} = (P_c + P_t)T_{ac}$. Since the downlink data path is only used for transmission of command signals, we assume that the total energy consumption (in both RF transmission and circuits) during the downlink transmission period is negligible compared to that of the uplink case. The energy consumption in the sleep mode period is given by $E_{sl} = P_{sl}T_{sl}$, where P_{sl} is the corresponding power consumption. The present state-of-the art in implantable devices aims to keep a very low sleep mode leakage current (coming from the CMOS circuits in the IBS), resulting in $P_{sl} \approx 0$ when compared to the power consumption in the active mode duration. This assumption is used in many studies on the energy efficiency of wireless sensor networks (e.g., see [20], [21]). As a result, the *energy efficiency*, referred to as the performance metric of the proposed implant WBAN, can be measured by the total energy consumption during the uplink transmission interval and corresponding to L -bit message \mathbb{M}_L as follows:

$$E_L = (P_c + P_t)T_{ac} + P_{tr}T_{tr}, \quad (1)$$

where P_{tr} is the circuit power consumption during the transient mode period. It is seen from (1) that the active mode duration T_{ac} is an influential factor in energy saving, as E_L is a monotonically decreasing function of T_{ac} .

III. IN-BODY CHANNEL MODEL

An important element in the optimum design of implantable devices is to characterize a realistic channel model for the human body. For this purpose, we first study the tissue characteristics and their effects on the signal propagation loss across the human body over the MICS frequency band.

Human body is an inhomogeneous and lossy medium which consists of various tissue layers with different thicknesses and their own unique electrical characteristics over the frequency of interest. Each tissue layer absorbs the electromagnetic energy which results in a considerable attenuation of ultra low power waves propagated from the IBS to the CCU. In this work, we consider three different tissue layers composed of muscle, fat and skin, approximating the structure of a human torso for modeling the channel between the IBS and the CCU. This model is used in many recent published works (e.g., see [4], [13]). Table II details the frequency-dependent permittivity ϵ_r and conductivity σ of the aforementioned tissue of an adult male at 403.5 MHz [4], [22]. The electrical properties of the body tissues help in designing proper antennas for implantable devices, and the in-body path loss channel model. The physical radio propagation with implanted antennas through human tissues has been extensively studied in the open literature over the past few years (e.g., see [16] and its references), and is out of scope of this work. Derivation of the exact expression for

TABLE II
ELECTRICAL PROPERTIES OF THE MAIN TISSUE LAYERS OF AN ADULT HUMAN BODY AT 403.5 MHz

Tissue	ϵ_r	σ (S/m)
Skin (Dry)	46.706	0.6895
Fat	5.5783	0.0411
Muscle	57.10	0.7972

TABLE III
PARAMETERS FOR THE PATH LOSS MODEL OF A HUMAN BODY AT 403.5 MHz [23]

Tissue	\mathcal{L}_0 (dB)	η	σ_χ (dB)
Deep Tissue	47.14	4.26	7.85
Near Surface	49.81	4.22	6.81

the in-body channel model is extremely difficult. Reference [23] uses a sophisticated 3D virtual simulation platform to extract a simple statistical path loss model for the in-body channel over the MICS frequency band. We denote P_t and P_r as the transmitted and the received signal powers for the uplink, respectively. In addition, it is assumed that the IBS and the CCU are separated by distance d . In this case, the gain factor \mathcal{L}_d for a η^{th} -power path loss channel is expressed as

$$\mathcal{L}_d = \frac{P_t}{P_r} = \mathcal{L}_0 \left(\frac{d}{d_0} \right)^\eta \chi_r \quad (2)$$

$$\mathcal{L}_d(\text{dB}) = \mathcal{L}_0(\text{dB}) + 10\eta \log_{10} \left(\frac{d}{d_0} \right) + \chi_r(\text{dB}), \quad (3)$$

where \mathcal{L}_0 is the gain factor at the reference distance d_0 which is specified by the transmitter and the receiver antenna gains and wavelength λ , η is the path loss exponent, and $\chi_r \sim N(0, \sigma_\chi^2)$ is a normal random variable which represents the deviation caused by different tissue layers (e.g., skin, muscle, fat) and the antenna gain in different directions [23]. Table III shows the parameters for the statistical path loss model corresponding to the channel between the IBS and the CCU for near-surface (e.g., cardiac pacemaker located in the left pectoral region) and deep tissue (e.g., digestive endoscopy) applications.

For the above channel model and denoting $s_i(t)$ as the RF transmitted signal with energy E_t , the received signal at the CCU is given by $r_i(t) = \frac{1}{\sqrt{\mathcal{L}_d}} s_i(t) + z_i(t)$, where $z_i(t)$ is the AWGN at the CCU with two-sided power spectral density given by $\frac{N_0}{2}$. It should be noted that the power spectral density of the noise introduced by the receiver front-end at the CCU is calculated by $N_0 = \kappa T_0 10^{\frac{NF}{10}}$ (W/Hz), where $\kappa = 1.3806503 \times 10^{-23}$ is the Boltzmann constant, T_0 is the body temperature (in Kelvin) and NF is the noise figure of the receiver at the CCU. Under the above considerations, the Signal-to-Noise Ratio (SNR), denoted by γ , can be computed as $\gamma = \frac{E_t}{\mathcal{L}_d N_0}$.

IV. UNCODED FSK MODULATION

A challenge that arises with implantable medical devices is to design a small size and ultra low power transceiver which operates efficiently over the MICS frequency band. With this observation in mind, finding the energy efficient modulation

with low-complexity implementation is a crucial task in the design of tiny biosensors. Broadly, the transceivers can be divided into two categories based on the following modulation techniques: *i)* sinusoidal carrier-based and *ii)* UWB schemes. UWB modulation schemes such as OOK benefit in very simple design in transmitters along with low power consumption in circuits. However, according to the FCC regulations for UWB systems [15], UWB technology is used solely for transmitting information over a wide bandwidth at least 500 MHz, which is much wider than the bandwidth used in the MICS standard. In addition, the 3-10 GHz frequency band used for UWB systems is far from the 402-405 MHz frequency range in implantable devices. On the other hand, sinusoidal carrier-based modulation schemes can meet the MICS specifications, in particular the frequency band 402-405 MHz and the data rate of at least 250 kbps. Among various sinusoidal carrier-based modulation techniques, Frequency Shift Keying (FSK), known as the *green modulation*, has been found to provide a good compromise between high data rate, simple radio architecture, low power consumption, and requirements on linearity of the modulation scheme [24], [25]. Note that more complex modulation schemes such as QAM which are often used in conventional RF communication applications are not easily amenable to the ultra low power communication demanded by implantable medical devices, due to higher power consumption.

An FSK scheme is a very simple and low power structure which is widely utilized in energy-constrained wireless applications [12], [25] and the IEEE 802.15.6 WPAN Work Group (WG) (e.g., see [19]). In an M -ary FSK modulation scheme, M orthogonal carriers are mapped into $b = \log_2 M$ bits. The main advantage of this orthogonal signaling is that the received signals at the CCU do not interfere with one another in the process of detection at the receiver. An MFSK modulator benefits in using the Direct Digital Modulation (DDM) approach, meaning that modulation is implemented digitally inside the frequency synthesizer. This property makes MFSK consume very little power and has a faster start-up time than other sinusoidal carrier-based modulations. The output of the frequency synthesizer can be frequency modulated and controlled simply by b bits in the input of a “digital control” unit. The modulated signal is then filtered again, amplified by the Power Amplifier (PA), and finally transmitted across the human body channel. We denote the power consumption of the frequency synthesizer, filters and the power amplifier as P_{Sy} , P_{Filt} and P_{Amp} , respectively. In this case, the circuit power consumption of the IBS is given by $P_{ct} = P_{Sy} + P_{Filt} + P_{Amp}$, where $P_{Amp} = \alpha P_t$ and the value of α is determined based on type of the power amplifier. Also, denoting P_{LNA} , P_{Filt} , P_{ED} , P_{IFA} and P_{ADC} as the power consumption of Low-Noise Amplifier (LNA), filters, envelope detector, IF amplifier and ADC, respectively, the power consumption of the CCU circuitry with the Non-Coherent M -ary FSK (NC-MFSK) can be obtained as $P_{cr} = P_{LNA} + M \times (P_{Filt} + P_{ED}) + P_{IFA} + P_{ADC}$ [25]. In addition, it is shown that the energy consumption during T_{tr} is obtained as $P_{tr} T_{tr} = 1.75 P_{Sy} T_{tr}$ [25].

The energy and bandwidth efficiency of FSK have been extensively studied in the literature (e.g., see [20], [25]). Table

IV summarizes the parameters of an uncoded NC-MFSK over an AWGN channel with path loss which is the same as the channel model for the human body. There are some interesting points extracted from Table IV.

i) It is observed that the active mode duration T_{ac} is a monotonically increasing function of constellation size M , when L and B are fixed. Since, we are interested in having T_{ac} as small as possible for energy saving (according to (1)), as well as having a low complexity detector at the CCU, the higher order of constellation size M for the above NC-MFSK is not desirable. Another advantage of using a lower order of M is to improve the bandwidth efficiency which is the main concern in MFSK scheme. Of course, a good spectral efficiency is achieved using Minimum-Shift Keying (MSK) and in particular Gaussian Minimum-Shift Keying (GMSK) as a special case of FSK.

ii) Using $B = \frac{M}{2T_s} = 300$ KHz, the data rate is obtained as $R = \frac{b}{T_s} = 2B \frac{\log_2 M}{M}$ which must be greater than 250 kbps according to the MICS specifications in Table I. It is seen that only $M = 2$ and $M = 4$ satisfy this requirement emphasizing using the lower order of M for MFSK modulation scheme.

iii) Assuming M and L are fixed, it is revealed from $T_{ac} = \frac{ML}{2B \log_2 M}$ that the active mode duration in the IBS with $B = 300$ KHz is approximately 20% of T_{ac} for the wireless sensor applications with the same NC-MFSK structure, where they use the bandwidth $B = 62.5$ KHz according to Table I. Thus, an 80% energy saving is achievable for implantable devices with the MICS standard as compared to the IEEE 802.15.4 physical layer protocol with the same structure used for sensor networking applications. This interesting result justifies the reason of using a wider bandwidth in the MICS standard than that of the IEEE 802.15.4 protocol for WSNs.

Now, we are ready to derive the total energy consumption of an NC-MFSK based on the results in Table IV. Recall from $E_t = P_t T_s \approx 2\mathcal{L}_d N_0 \ln \frac{M}{4P_b}$, we have

$$P_t T_{ac} = E_t \frac{T_{ac}}{T_s} = 2 \frac{\mathcal{L}_d N_0 L}{\log_2 M} \ln \frac{M}{4P_b}. \quad (4)$$

Substituting (4), $T_{ac} = \frac{ML}{2B \log_2 M}$ and $P_{Amp} = \alpha P_t$ in (1), the total energy consumption of an NC-MFSK scheme for transmitting L bits during the uplink transmission interval and for a given P_b is obtained as

$$E_L = 2(1 + \alpha) \mathcal{L}_d N_0 \frac{L}{\log_2 M} \ln \frac{M}{4P_b} + (P_c - P_{Amp}) \frac{ML}{2B \log_2 M} + 1.75 P_{Sy} T_{tr}. \quad (5)$$

In transmitting the vital physiological signs of patients, the BER should be as small as possible. Since, the BER is a function of the received SNR and to maintain the BER in a specific limit, one would increase the transmit signal power which is not desirable in ultra low power implantable medical devices with EIRP=-16 dBm. One practical solution to avoid an increase in the transmit power is to use channel coding schemes. For energy optimal designs, however, the impact of channel coding on the energy efficiency computed in (5) must be considered as well. It is a well known fact that channel coding is a fundamental approach used to improve the link

TABLE IV
PARAMETERS FOR AN UNCODED NC-MFSK OVER AWGN CHANNEL WITH PATH LOSS

Parameter	Formula
Transmitted Signal	$s_i(t) = \sqrt{\frac{2E_t}{T_s}} \cos(2\pi(f_0 + i\Delta f)t), i = 0, 1, \dots, M - 1$
Symbol Duration	T_s
First Carrier Frequency	f_0
Minimum Carrier Separation	$\Delta f = \frac{1}{2T_s}$
Channel Bandwidth (Hz)	$B \approx M \times \Delta f = \frac{M}{2T_s}$
Data Rate (b/s)	$R = \frac{b}{T_s}$
Bandwidth Efficiency (b/s/Hz)	$B_{eff} = \frac{R}{B} = \frac{2 \log_2 M}{M}$
Active Mode Duration	$T_{ac} = \frac{L}{b} T_s = \frac{ML}{2B \log_2 M}$
Bit Error Rate	$P_b \leq \frac{M}{4} e^{-\frac{\gamma}{2}} = \frac{M}{4} e^{-\frac{E_t}{2N_0 L_d}}$
Transmit Energy Per Symbol	$E_t = P_t T_s \approx 2\mathcal{L}_d N_0 \ln \frac{M}{4P_b}$
Power Consumption of IBS Circuitry	$P_{ct} = P_{Sy} + P_{Filt} + P_{Amp}$
Power Consumption of CCU Circuitry	$P_{cr} = P_{LNA} + M \times (P_{Filt} + P_{ED}) + P_{IFA} + P_{ADC}$

reliability using redundant information bits along with the transmitter energy saving due to the providing of coding gain [26]. However, the energy saving comes at the cost of extra energy consumed in transmitting the redundant bits in codewords as well as the additional energy consumption in the process of encoding/decoding. For a certain transmission distance d , if these extra energy consumptions outweigh the transmit energy saving due to the channel coding, the coded system would not be energy efficient compared with an uncoded system. In the subsequent sections, we will argue the above issue for LT codes and show that the LT coded NC-MFSK surpasses the distance constraint (or equivalently the dynamic environment between the IBS and the CCU) achieving a given BER in the proposed system.

V. ENERGY EFFICIENCY AND RELIABILITY OF LT CODES

The task of the IBS is to communicate vital signs of the patient as accurately as possible to the CCU, due to the potentially life-threatening situations in patient monitoring. This is called data *reliability* which depends strongly on the channel conditions. Reliability in a wireless network, in general, is evaluated in terms of the probability of packet loss or the probability of a data packet being delivered correctly to the receiver. Enhanced reliability is achieved by adding redundant bits in data packets in the FEC coding stage at the cost of an extra power consumption. Thus, there exists a tradeoff between a higher reliability and a lower power consumption in using FEC codes. Finding a proper FEC coding scheme for balancing energy consumption, complexity and data reliability is a challenging task in designing implant WBANs; in particular, when data transfer across tissues is susceptible to loss and transmission errors. The emerging LT codes (as the first practical rateless codes) have exhibited strong capabilities in reaching the above targets over the lossy channel model for the human body for the following reasons:

i) Optimality: It is shown in [18] that LT codes are near optimal erasure correcting codes without the knowledge of the channel erasure rate at the transmitter.

ii) Code-Rate Flexibility: To ensure reliable communication across tissues, a sufficient amount of energy must arrive at the CCU. For fixed-rate codes (e.g., linear block codes),

this may be done by adaptively adjusting the transmitted power based on the channel condition. Such an adaptive power control is not feasible for the IBS due to the complexity concerns for implantable medical devices. LT codes, on the other hand, can adapt to different channel realizations via changing the code rate (instead of the power control) to achieve a certain BER. In addition, they have the capability of high degree of reliability in correct delivery of data packets over a lossy channel.

iii) Simplicity: The LT encoding process is extremely simple when compared with some traditional block codes such as Reed Solomon (RS) codes and Low-Density-Parity-Check (LDPC) codes, and has a tight power budget. In addition, most of the complexity of an LT code (i.e., message passing decoder) is pushed to the CCU which has effectively unlimited power and computational resource.

The above capabilities of LT codes have removed the critical obstacles of using the classical fixed-rate codes (e.g., block and convolutional codes), where the transferred data experience different packet loss or error rates in different SNRs due to the dynamic channel conditions for the human body. In this section, we briefly introduce some basic concepts and definitions for the LT codes. Then, we analyze the energy efficiency and the reliability of LT coded NC-MFSK for the proposed implant WBAN. To get more insight into how LT codes affect the circuit and RF signal energy consumptions in the system, we modify the energy concepts in Section IV, in particular, the total energy consumption expression in (5) based on the LT coding gain and code rate.

Following the notation of [27], an LT code is specified by the number of input bits k and the output-node degree distribution $\Omega(x) = \sum_{i=1}^k \Omega_i x^i$, where Ω_i , $i = 1, \dots, k$, denotes the probability that an output node has degree i . Without loss of generality and for ease of our analysis, we assume that a finite k -bit message $\mathbb{B}_1 = \{m_i\}_{i=1}^k \in \mathbb{M}_L$ is encoded to the codeword $\mathbb{C}_1 = \{a_j\}_{j=1}^n$ with $\Omega(x) : \{m_i\}_{i=1}^k \rightarrow a_j$, $j = 1, \dots, n$. More precisely, each single coded bit a_j is generated based on the encoding protocol proposed in [18]: *i)* randomly choose a degree $1 \leq \mathcal{D} \leq k$ from a priori known degree distribution $\Omega(x)$, *ii)* using a uniform distribution, randomly choose \mathcal{D} distinct input bits, and calculate the

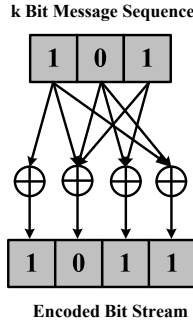


Fig. 3. Factor graph of an LT code with $k = 3$ and $n = 4$.

encoded bit a_j as the XOR-sum of these \mathcal{D} bits. The above encoding process defines a *factor graph* connecting encoded nodes to input nodes (see, e.g., Fig. 3). It is seen that the LT encoding process is extremely simple and the encoder has a much lower computational burden than the block codes. For instance, the complexity of the LT codes is of order $O(n \log n)$ compared to $O(n^2)$ for RS codes used in WiMAX in the IEEE 802.16 standard. This low complexity comes from exploiting XOR operations in LT codes (unlike field operations used for RS codes). Thus, one can with a good approximation assume that the energy consumption of an LT encoder is negligible compared to the other circuit components in the IBS. As a result, the energy cost of the IBS circuitry with the LT coded NC-MFSK scheme is approximately the same as that of the uncoded one.

One inherent property of LT codes is that they can vary their codeword block lengths to match a wide range of possible channel conditions. In fact, for a specific value of SNR, $a_n \in \mathbb{C}_1$ is the last bit generated at the output of the LT encoder before receiving the acknowledgement signal from the CCU in the uplink path indicating termination of a successful decoding process. This is in contrast to classical linear block and convolutional codes, in which the codeword block length is fixed. As a result, the LT code rate, denoted by $R_c = \frac{k}{n}$, displays a random variable indicating the rateless behavior of the LT code.

We now turn our attention to the LT code design for the augmentation protocol. As seen in the LT encoding process, the output-node degree distribution $\Omega(x)$ is the most influential factor in the complexity of the LT code. Typically, optimizing $\Omega(x)$ for a specific wireless channel is a crucial task in designing LT codes. In this work, we use the following output-node degree distribution which was optimized for a BSC using a hard-decision decoder [28], [29]:

$$\begin{aligned} \Omega(x) = & 0.00466x + 0.55545x^2 + 0.09743x^3 + \\ & 0.17506x^5 + 0.03774x^8 + 0.08202x^{14} + \\ & 0.01775x^{33} + 0.02989x^{100}. \end{aligned} \quad (6)$$

The LT decoder at the CCU is able to reconstruct the entire k -bit message \mathbb{B}_1 with a high degree of reliability after receiving any $(1+\epsilon)k$ bits in its buffer, where ϵ depends upon the LT code design and channel condition [27]. In this work, we assume that the CCU recovers a k -bit message \mathbb{B}_1 using a simple hard-decision “ternary message passing” decoder in a

nearly identical manner to the “Algorithm E” decoder in [30] for Low-Density Parity-Check (LDPC) codes. Description of the *ternary message passing* decoding is out of scope of this work, and the reader is referred to Chapter 4 in [28] for more details. It should be noted that the degree distribution $\Omega(x)$ in (6) was optimized for a ternary decoder in a BSC and we are aware of no better $\Omega(x)$ for the ternary decoder in AWGN channels.

To analyze the energy efficiency of the LT coded NC-MFSK scheme, we note that the number of transmitted bits during the uplink transmission period is increased from the L -bit uncoded message to $\frac{L}{R_c} = \frac{L}{k}n$ bits coded one. In order to keep the bandwidth of the coded system the same as that of the uncoded case, we must keep the information transmission rate constant, i.e., the symbol duration T_s of uncoded and coded NC-MFSK would be the same. According to Table IV, however, the active mode duration increases from $T_{ac} = \frac{L}{b}T_s$ in the uncoded system to

$$T_{ac,c} = \frac{L}{bR_c}T_s = \frac{T_{ac}}{R_c} = \frac{ML}{2R_cB \log_2 M}, \quad (7)$$

for the LT coded case, where we use $T_{ac} = \frac{ML}{2B \log_2 M}$ in Table IV. An interesting point raised from (7) is that $T_{ac,c}$ is a function of the random variable R_c which results in an inherent adaptive duty-cycling for power management in each channel condition. To compute the total energy consumption of coded scheme, we use the fact that channel coding can reduce the required SNR value to achieve a given BER. Denoting $\gamma = \frac{E_t}{\mathcal{L}_d N_0}$ and $\gamma_c = \frac{E_{t,c}}{\mathcal{L}_d N_0}$ as the SNR of uncoded and coded schemes, respectively, the *coding gain* \mathcal{G}_c (expressed in dB) is defined as the difference between the values of γ and γ_c required to achieve a certain BER, where $E_{t,c} = \frac{E_t}{\mathcal{G}_c}$. Taking this into account, the proposed implant system with LT codes benefits in transmission energy saving specified by \mathcal{G}_c . Tables V and VI (also see Fig. 4) give the LT code rates and the corresponding coding gains of LT coded NC-MFSK scheme using $\Omega(x)$ in (6) and for $M = 2$ and 4 and different values of BER. It is observed that the LT code is able to provide a large value of coding gain \mathcal{G}_c given BER, but this gain comes at the expense of a very low code rate, which means many additional code bits need to be sent. This results in higher energy consumption per information bit. An interesting point extracted from Fig. 4 is the flexibility of the LT code to adjust its rate (and its corresponding coding gain) to suit channel conditions in implant WBANs. For instance, in the case of favorable channel conditions, the LT coded NC-MFSK is able to achieve a code rate approximately equal to one with $\mathcal{G}_c \approx 0$ dB in the BER=10⁻³, which is similar to the case of uncoded NC-MFSK. The effect of LT code rate flexibility on the total energy consumption is also observed in the simulation results in the subsequent section.

To get more insight into the results of Tables V and VI, we illustrate the LT code rates versus SNR for several different values of BER for the cases where $M = 2$ and $M = 4$ in Fig. 5. These results were obtained by evaluating the performance of the LT code using density evolution, as described in [28]. An interesting phenomenon exhibited in the figure is that the curves tend to converge for a given M as SNR decreases.

TABLE V
CODE RATE AND CODING GAIN(dB) OF LT CODED NC-MFSK OVER
AWGN FOR DIFFERENT VALUES OF P_b AND $M=2$.

SNR (dB)	$P_b = 10^{-3}$		$P_b = 10^{-4}$		$P_b = 10^{-5}$	
	R_c	\mathcal{G}_c	R_c	\mathcal{G}_c	R_c	\mathcal{G}_c
3	0.1624	7.94	0.1624	9.31	0.1624	10.35
4	0.2346	6.94	0.2346	8.31	0.2346	9.35
5	0.3248	5.94	0.3248	7.31	0.3101	8.35
6	0.4304	4.94	0.4304	6.31	0.3889	7.35
7	0.5438	3.94	0.5438	5.31	0.4699	6.35
8	0.6513	2.94	0.6513	4.31	0.5458	5.35
9	0.7378	1.94	0.7378	3.31	0.6075	4.35
10	0.8003	0.94	0.8003	2.31	0.6479	3.35
11	0.8650	-0.06	0.8419	1.31	0.6671	2.35
12	0.9229	-1.06	0.8488	0.31	0.6732	1.35
13	0.9553	-2.06	0.8498	-0.69	0.6748	0.35
14	0.9685	-3.06	0.8508	-1.69	0.6754	-0.65

TABLE VI
LT CODE RATE AND CODING GAIN(dB) OF LT CODED NC-MFSK OVER
AWGN FOR DIFFERENT VALUES OF P_b AND $M=4$.

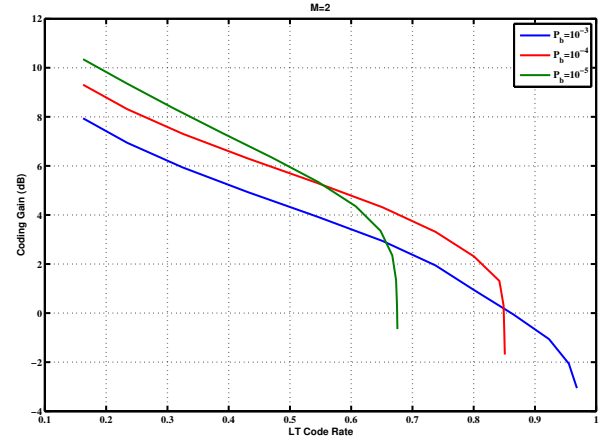
SNR (dB)	$P_b = 10^{-3}$		$P_b = 10^{-4}$		$P_b = 10^{-5}$	
	R_c	\mathcal{G}_c	R_c	\mathcal{G}_c	R_c	\mathcal{G}_c
7	0.1613	7.37	0.1613	8.64	0.1613	9.62
8	0.2380	6.37	0.2380	7.64	0.2380	8.62
9	0.3365	5.37	0.3365	6.64	0.3190	7.62
10	0.4525	4.37	0.4525	5.64	0.4051	6.62
11	0.5754	3.37	0.5754	4.64	0.4925	5.62
12	0.6885	2.37	0.6885	3.64	0.5709	4.62
13	0.7681	1.37	0.7681	2.64	0.6289	3.62
14	0.8343	0.37	0.8343	1.64	0.6605	2.62
15	0.9032	-0.63	0.8468	0.64	0.6720	1.62
16	0.9486	-1.63	0.8498	-0.36	0.6746	0.62
17	0.9654	-2.63	0.8503	-1.36	0.6748	-0.38

This result comes from the fact that for large block lengths, LT codes exhibit a decoding threshold in much the same way that LDPC codes do. Essentially, this means that for a particular SNR there exists a threshold rate above which the LT code will not successfully decode. At or below this threshold rate, the LT code *will* decode and the decoded message will have a particular BER. As the rate is further decreased, the BER will decrease in a continuous manner. Thus, there exists a discontinuity in the BER at the decoding threshold, where the BER of an LT decoded message drops from being very high (i.e., many errors since the LT decoder failed to converge to a solution for rates above the threshold) to very low (i.e., the LT code converged at a successful solution for rates below the threshold). This discontinuity is more pronounced at lower SNR, meaning that the BER values of 10^{-3} , 10^{-4} , and 10^{-5} all appear to occur at the same points on the rate-SNR curve.

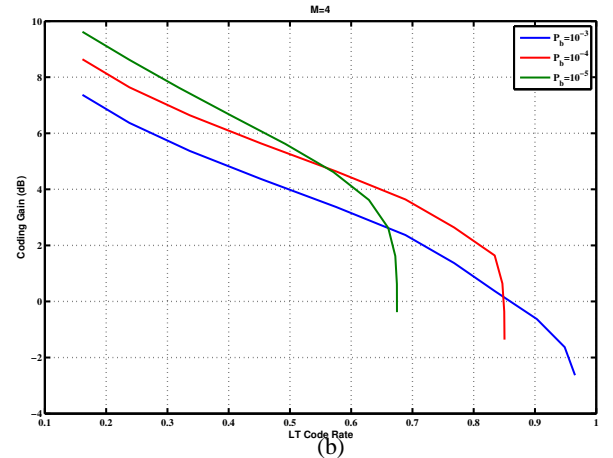
We denote E_{enc} and E_{dec} as the computation energy of the encoder and decoder for each information bit, respectively. Thus, the total computation energy cost of the coding components for $\frac{L}{R_c}$ bits is obtained as $L \frac{E_{enc} + E_{dec}}{R_c}$. Substituting $E_t = 2\mathcal{L}_d N_0 \ln \frac{M}{4P_b}$ in $E_{t,c} = \frac{E_t}{\mathcal{G}_c}$ and using (7), the total RF signal energy consumption during active mode duration $T_{ac,c}$ for the coded case is given by

$$P_{t,c} T_{ac,c} = E_{t,c} \frac{T_{ac,c}}{T_s} = 2 \frac{\mathcal{L}_d N_0}{\mathcal{G}_c} \frac{L}{R_c \log_2 M} \ln \frac{M}{4P_b}. \quad (8)$$

Substituting (7) and (8) in (1), and using the fact that $P_{Amp} = \alpha P_{t,c}$, the total energy consumption of transmitting $\frac{L}{R_c}$ bits during the uplink transmission period for an LT coded



(a)



(b)

Fig. 4. LT coding gain versus LT code rate for different values of BER and for a) $M = 2$, b) $M = 4$.

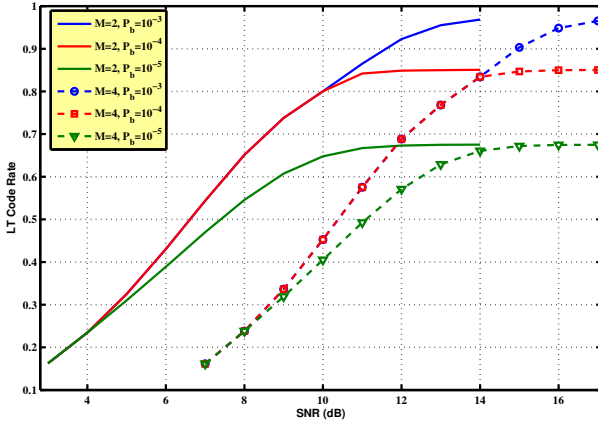
NC-MFSK scheme, denoted by $E_{L,c}$, and for a given P_b is obtained as

$$E_{L,c} = 2(1 + \alpha) \frac{\mathcal{L}_d N_0}{\mathcal{G}_c} \frac{L}{R_c \log_2 M} \ln \frac{M}{4P_b} + (P_c - P_{Amp}) \frac{ML}{2R_c B \log_2 M} + 1.75 P_{Sy} T_{tr} + L \frac{E_{enc} + E_{dec}}{R_c}, \quad (9)$$

where the goal is to minimize $E_{L,c}$ in each distance d , in terms of modulation and coding parameters. Although, higher reliability (corresponding to the lower BER) results in an increase in the total energy consumption $E_{L,c}$, the effect of the coding gain \mathcal{G}_c and the code rate R_c on $E_{L,c}$ for a given P_b should be considered as well.

VI. NUMERICAL EVALUATION

This section presents some numerical evaluations using realistic parameters from the MICS standard and state-of-the-art technology to confirm the reliability and energy efficiency analysis of uncoded and LT coded NC-MFSK schemes discussed in Sections IV and V. We assume that the NC-MFSK modulation scheme operates in the carrier frequency

Fig. 5. LT code rate versus SNR for different values of BER and $M=2, 4$.TABLE VII
SYSTEM EVALUATION PARAMETERS

$B = 300$ KHz	$T_{tr} = 5$ μ s	$P_{ADC} = 7$ mW
$d_0 = 30$ mm	$P_{Sy} = 10$ mW	$P_{LNA} = 9$ mW
$N_0 = -110.91$ dBm	$P_{Filt} = 2.5$ mW	$P_{ED} = 3$ mW
$T_L = 1.4$ sec	$P_{Filt} = 2.5$ mW	$P_{IFA} = 3$ mW

$f_0 = 403.5$ MHz according to the frequency band requirement in the MICS standard. As shown in Section IV, we only consider the constellation sizes $M = 2, 4$. We assume that in each period T_L , the sensed data frame size $L = 1024$ bytes (or equivalently $L = 8192$ bits) is generated, where T_L is assumed to be 1.4 seconds. The channel bandwidth is assumed to be $B = \frac{M}{2T_s} = 300$ KHz, according to Table I. As a result, the symbol duration T_s for $M = 2$ and $M = 4$ is obtained as 3.33 μ s and 6.67 μ s, respectively. Also, the data rate $R = \frac{b}{T_s}$ for both $M = 2, 4$ will be 300 kbps which satisfies the data rate requirement in Table I. Assuming $T_0 = 310^\circ K$ for the body temperature and $NF=8$ dB, the total noise power at the bandwidth $B = 300$ KHz is obtained as $N_0 = \kappa B T_0 10^{NF/10} = -110.91$ dBm. Table VII summarizes the system parameters for simulation. The results in Tables III-VI are also used to compare the energy efficiency of uncoded and LT coded NC-MFSK schemes. In addition, the current simulation is based on the values in Table III for the two following scenarios: *i*) near surface with the distance range of $d_0 = 30$ mm to 100 mm and *ii*) deep tissue where the distance d varies between 100 mm and 300 mm. For this purpose, it is assumed that the skin varies in thickness from 0.5 mm to 6 mm [31] and the muscle thickness varies in the range of 13-40 mm according to the MRI measurements in [32]. Furthermore, we assume that the fat thickness ranges from 0-250 mm for thin or obese patients. In order to estimate the computation energy of the channel coding, we use the ARM7TDMI core which is the industry's most widely used 32-bit embedded RISC microprocessor for an accurate power simulation [33].

Fig. 6 shows the total energy consumption versus distance d for the optimized LT coded NC-MFSK compared to the

optimized uncoded NC-MFSK for the cases $P_b = 10^{-3}$ and $P_b = 10^{-5}$, and for the proposed three different tissue layers with the aforementioned thicknesses. The optimization is performed over M and the parameters of coding scheme in Tables V and VI. For the case of $P_b = 10^{-3}$, it is revealed from Fig. 6-a that for distance d less than the threshold level $d_T \approx 70$ mm (near surface scenario), the total energy consumption of optimized uncoded NC-MFSK is less than that of the coded NC-MFSK schemes. However, the energy gap between the LT coded and uncoded approaches is negligible as expected. For $d > d_T$ which covers the deep tissue scenario, the LT coded NC-MFSK scheme is more energy efficient than the uncoded one, in particular when d grows. This result comes from the high coding gain capability of LT codes. An interesting phenomenon exhibited in Fig. 6-a is that the optimized LT coded NC-MFSK surpasses the distance constraint in implant WBAN applications. In addition, the flexibility of the LT code rate (and the corresponding LT coding gain) allows the system to adjust its duty-cycling for power management and to suit to different channel conditions for the human body for any distance d .

In the case of $P_b = 10^{-5}$ as depicted in Fig. 6-b, the uncoded NC-MFSK scheme is preferable to use for $d < d_T \approx 120$ mm which corresponds to the near-surface applications. This result follows from the maximum code rate of $R_c \approx 0.675$ for both $M = 2$ and $M = 4$ in $P_b = 10^{-5}$. However, for the deep tissue applications where $d > d_T \approx 120$ mm, the optimized LT coded NC-MFSK is much more energy efficient than the uncoded case.

It is concluded from the above observations that the threshold level d_T for a certain BER is a fundamental parameter in the physical layer design of implant WBANs, as it determines “when the LT codes are energy efficient” in the proposed wireless biomedical implant system. The parameter d_T is obtained when the total energy consumptions of coded and uncoded systems become equal. Using $\mathcal{L}_d = \mathcal{L}_0 \left(\frac{d}{d_0}\right)^\eta \chi_r$, and the equality between (5) and (9) for uncoded and LT coded NC-MFSK, we have

$$d_T = d_0 \left[\frac{M(\mathcal{P}_c - \mathcal{P}_{Amp})}{4(1 + \alpha)N_0 B \mathcal{L}_0 \chi_r \ln\left(\frac{M}{4P_b}\right)} \frac{\mathcal{G}_c(1 - R_c)}{\mathcal{G}_c R_c - 1} \right]^{\frac{1}{\eta}}.$$

It can be seen from the above equation that a decrease in the P_b results in an increase in the d_T as observed in Fig. 6. In addition, the growth rate of the energy consumption of the LT codes for deep tissue applications (i.e., $d > d_T$) is much smaller than that of the uncoded one when P_b decreases (equivalent to the higher reliability).

Remark: As discussed previously, the proposed LT coded scheme benefits in adjusting the coding parameters in each channel realization or equivalently each distance d to minimize the total energy consumption. For this case, as long as the CCU collects a sufficient number of bits, it will be able to decode the original message. Indeed, only the CCU needs to be aware of the channel conditions. The IBS, as the transmitter, always sends an LT encoded stream using constant modulation and power, and the receiver alone determines how many bits to

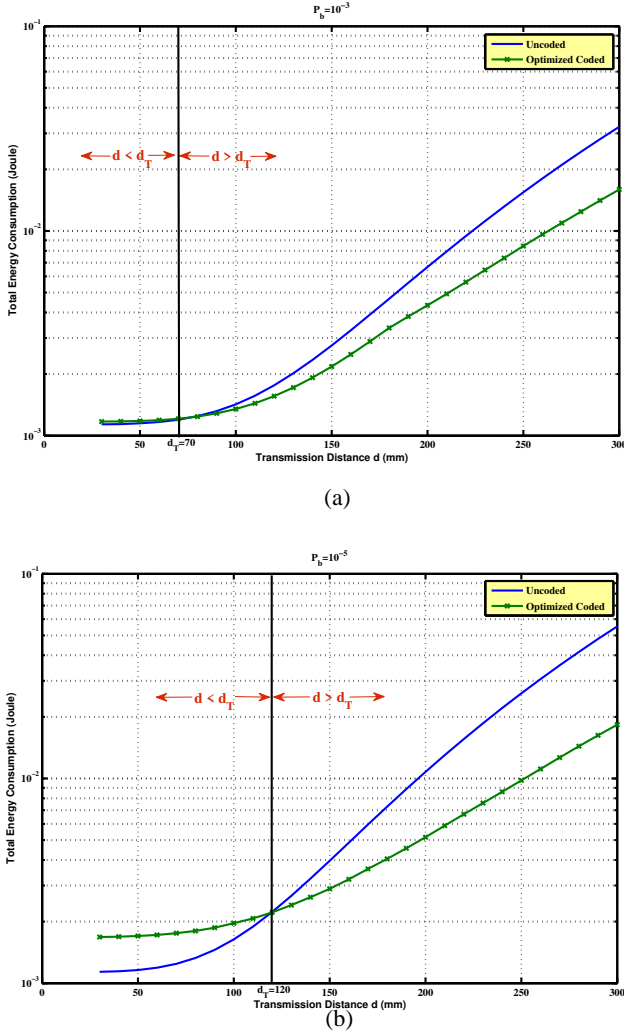


Fig. 6. Total energy consumption of uncoded and optimized LT coded NC-MFSK versus d for a) $P_b = 10^{-3}$ b) $P_b = 10^{-5}$.

collect, their reliability, and ultimately decodes the message. Thus, the transmitter does not need to change coding rate, because the rate is determined entirely by how many bits it collects based on the channel quality. There is no channel information required at the transmitter which reduces the complexity and cost in implementation.

In contrast to the ARQ scheme, the only feedback in the LT coded system is a single message from transmitter to receiver (at the end of a long block) indicating that a sufficient number of bits have been collected and it is time to move on to the next data block. This is not an ARQ scheme, but it is more similar to an incremental redundancy scheme whereby a message is encoded using a rate-compatible punctured code.

In addition, a nice feature about the optimized LT code as opposed to the punctured codes is that there is truly no “minimum rate” at which the code can operate. More precisely, we can choose a code that allows us to drop the rate as low as we need. With punctured LDPC, it is reported in [34] that depending upon the operating range, rate, etc. the LDPC performance drops off dramatically beyond a certain rate threshold—a phenomenon not observed by the rateless

codes.

VII. CONCLUSION

In this paper, we presented an augmentation protocol for the physical layer of the MICS standard with focus on the energy efficiency and the reliability of LT coded NC-MFSK scheme over the MICS frequency band. It was shown that the proposed scheme provides an inherent adaptive duty-cycling for power management which comes from the flexibility of the LT code rate. Analytical results demonstrated that an 80% energy saving is achievable with the proposed protocol when compared to the IEEE 802.15.4 physical layer protocol with the same structure used for wireless sensor networks. Numerical results have shown a lower energy consumption keeping at the same time a higher degree of reliability in the LT coded NC-MFSK scheme for deep tissue scenarios when compared to the uncoded case. In addition, it was shown that the optimized LT coded NC-MFSK is capable to surpass the distance constraint in implantable medical devices for the $BER=10^{-3}$. In fact, since the efficiency of implantable medical devices is strongly related to the human body structure (e.g., obese or thin and tissue composition), the proposed scheme overcomes the patient’s vital information loss and errors, and operates in a high degree of accuracy over any dynamic channel conditions for the human body. The introduced protocol is unique in implant WBAN applications, as it has been explicitly designed with simplicity and flexibility in mind, and should be usable in current wireless medical networking hardware.

ACKNOWLEDGMENT

The authors would like to thank Ali Tawfiq (University of Toronto) for graciously editing this paper.

REFERENCES

- [1] R. Schmidt, T. Norgall, J. Mrsdorf, J. Bernhard, and T. von der Grn, “Body area network BAN: a key infrastructure element for patient-centered medical applications,” *Biomed Tech (Berl)*, vol. 47, pp. 365–368, Jan. 2002.
- [2] U. Varshney and S. Sneha, “Patient monitoring using ad hoc wireless networks: reliability and power management,” *IEEE Communications Magazine*, vol. 44, no. 4, pp. 49–55, April 2006.
- [3] E. Reusens, W. Joseph, B. Latr, B. Braem, G. Vermeeren, E. Tanghe, L. Martens, I. Moerman, and C. Blondia, “Characterization of on-body communication channel and energy efficient topology design for wireless body area networks,” *IEEE Trans. on Information Technology in Biomedicine*, vol. 13, no. 6, pp. 933–945, Nov. 2009.
- [4] K. Y. Yazdandoost and R. Kohno, “Body implanted medical device communications,” *IEICE Trans. on Commun.*, vol. E92-B, no. 2, pp. 410–417, Feb. 2009.
- [5] FCC, “Wireless Medical Telemetry,” Federal Communications Commission, Jan. 2000, online available at <http://wireless.fcc.gov>.
- [6] R. A. M. Receveur, F. W. Lindemans, and N. F. D. Rooij, “Microsystem technologies for implantable applications,” *Journal of Micromechanics and Microengineering*, vol. 17, no. 5, pp. R50–R80, May 2007.
- [7] “Federal Communications Commission (FCC), code of federal regulations (CFR), title 47 part 95, MICS band plan,” FCC, Washington, DC, March 2003, online available at <http://www.fcc.gov>.
- [8] IEEE Standards, “Part 15.4: Wireless Medium Access control (MAC) and Physical Layer (PHY) Specifications for Low-Rate Wireless Personal Area Networks (WPANs),” in *IEEE 802.15.4 Standards*, Sept. 2006.
- [9] “Range extension for IEEE 802.15.4 and ZigBee applications,” *FreeScale Semiconductor, Application Note*, Feb. 2007.

- [10] Q. Tang, N. Tummala, S. K. S. Gupta, and L. Schwiebert, "Communication scheduling to minimize thermal effects of implanted biosensor networks in homogeneous tissue," *IEEE Trans. on Biomedical Engineering*, vol. 52, no. 7, pp. 1285–1294, July 2005.
- [11] J.-Y. Oh, J.-H. Kim, H.-S. Lee, and J.-Y. Kim, "PSSK modulation scheme for high data rate implantable medical devices," *IEEE Trans. on Information Technology in Biomedicine*, vol. 14, no. 3, pp. 634–640, May 2010.
- [12] J. L. Bohorquez, A. P. Chandrakasan, and J. L. Dawson, "A 350 μ W CMOS MSK transmitter and 400 μ W OOK super-regenerative receiver for medical implant communications," *IEEE Journal of Solid-State Circuits*, vol. 44, no. 4, pp. 1248–1259, April 2009.
- [13] N. Cho, T. Roh, J. Bae, and H.-J. Yoo, "A planar MICS band antenna combined with a body channel communication electrode for body sensor network," *IEEE Trans. on Microwave Theory and Techniques*, vol. 57, no. 10, pp. 2515–2522, Oct. 2009.
- [14] M. R. Yuce, H. C. Keong, and M. S. Chae, "Wideband communication for implantable and wearable systems," *IEEE Trans. on Microwave Theory and Techniques*, vol. 57, no. 10, pp. 2597–2604, Oct. 2009.
- [15] I. Oppermann, M. Hamalainen, and J. Iinatti, *UWB Theory and Applications*, John Wiley and Sons, 2004.
- [16] A. Sani, A. Alomainy, and Y. Hao, "Numerical characterization and link budget evaluation of wireless implants considering different digital human phantoms," *IEEE Trans. on Microwave Theory and Techniques*, vol. 57, no. 10, pp. 2605–2613, Oct. 2009.
- [17] M. C. Vuran and I. F. Akyildiz, "Error control in wireless sensor networks: A cross layer analysis," *IEEE/ACM Trans. on Networking*, vol. 17, no. 4, pp. 1186–1199, Aug. 2009.
- [18] M. Luby, "LT codes," in *Proc. of the 43rd Annual IEEE Symposium on Foundations of Computer Science (FOCS)*, 2002, pp. 271–280.
- [19] Hind Chebbou *et al.*, "Proposal for Partial PHY and MAC including Emergency Management in IEEE802.15.6," May 2009, available at IEEE 802.15 WPAN TG6 in Body Area Network (BAN), <http://www.ieee802.org/15/pub/TG6.html>.
- [20] S. Cui, A. J. Goldsmith, and A. Bahai, "Energy-constrained modulation optimization," *IEEE Trans. on Wireless Commun.*, vol. 4, no. 5, pp. 2349–2360, Sept. 2005.
- [21] J. Abouei, J. D. Brown, K. N. Plataniotis, and S. Pasupathy, "On the energy efficiency of LT codes in proactive wireless sensor networks," to appear in *IEEE Transactions on Signal Processing*, 2011.
- [22] Institute for Applied Physics Italian National Research Council, "Dielectric properties of body tissues," FCC, Washington, DC, online available at <http://niremf.ifac.cnr.it>.
- [23] K. Sayrafian-Pour, W.-B. Yang, J. Hagedorn, J. Terrill, and K. Y. Yazdandoost, "A statistical path loss model for medical implant communication channels," in *Proc. IEEE International Symposium on Personal, Indoor and Mobile Radio Communications (PIMRC)*, Tokyo, Japan, Sept. 2009.
- [24] J. Abouei, K. N. Plataniotis, and S. Pasupathy, "Green modulation in dense wireless sensor networks," in *Proc. IEEE International Conference on Acoustics, Speech and Signal Processing (ICASSP'10)*, Dallas, Texas, USA, March 2010, pp. 3382–3385.
- [25] J. Abouei, K. N. Plataniotis, and S. Pasupathy, "Green modulations in energy-constrained wireless sensor networks," to appear in *IET Communications*, 2011.
- [26] J. G. Proakis, *Digital Communications*, New York: McGraw-Hill, forth edition, 2001.
- [27] A. Shokrollahi, "Raptor codes," *IEEE Trans. on Inform. Theory*, vol. 52, no. 6, pp. 2551–2567, June 2006.
- [28] J. D. Brown, *Adaptive Demodulation Using Rateless Erasure Codes*, Ph.D. Thesis, University of Toronto, 2008.
- [29] J. Abouei, J. D. Brown, K. N. Plataniotis, and S. Pasupathy, "On the energy efficiency of LT codes in proactive wireless sensor networks," in *Proc. IEEE Biennial Symposium on Communications (QBSC'10)*, Queen's University, Kingston, Canada, May 2010, pp. 114–117.
- [30] T. J. Richardson and R. L. Urbanke, "The capacity of low density parity-check codes under message-passing decoding," *IEEE Trans. on Inform. Theory*, vol. 47, no. 2, pp. 599–618, Feb. 2001.
- [31] Annette Wysocki, Thomas Mustoe, and Gregory Schultz, "Skin, molecular cell biology of," Wiley ebook, online available at <http://onlinelibrary.wiley.com/doi/10.1002/3527600906.mcb.200500065>, Sept. 2006.
- [32] A. C. Dupont, E. E. Sauerbrei, P. V. Fenton, P. C. Shragge, G. E. Loeb, and F. J. Richmond, "Real-time sonography to estimate muscle thickness: Comparison with MRI and CT," *Journal of Clinical Ultrasound*, vol. 29, no. 4, pp. 230–236, May 2001.
- [33] "ARM7TDMI Technical Reference Manual," Tech. Rep., available at <http://infocenter.arm.com/help/topic/com.arm.doc.ddi0210c/>.
- [34] E. Soljanin, N. Varnica, and P. Whiting, "Punctured vs rateless codes for hybrid ARQ," in *Proc. of IEEE Inform. Theory Workshop*, Punta del Este, Uruguay, March 2006.



Jamshid Abouei received the B.Sc. degree in electronics engineering and the M.Sc. degree in communication systems engineering (with the highest honor) both from the Isfahan University of Technology (IUT), Iran, in 1993 and 1996, respectively, and the Ph.D. degree in electrical engineering from the University of Waterloo in Waterloo, ON, Canada, in 2009.

From 1996 to 2004, he was a faculty member (lecturer) in the Department of Electrical Engineering, Yazd University, and from 1998 to 2004, he was a technical advisor and design engineer (part-time) in R&D center and cable design department in SGCC company. From 2009 to 2010, he was a Postdoctoral Fellow in the Multimedia Lab, in the Department of Electrical & Computer Engineering, at the University of Toronto, ON, Canada.

Currently, Dr Abouei is an Assistant Professor in the Department of Electrical & Computer Engineering, at the Yazd University, Iran. His research interests are in general areas of wireless ad hoc and sensor networks, with particular reference to energy efficiency and optimal resource allocation, multi-user information theory, cooperative communication in wireless relay networks, applications of game theory, and orthogonal codes in CDMA systems.

Dr Abouei has received numerous awards and scholarships, including FOE and IGSA awards for excellence in research in University of Waterloo, Canada, and MSRT Ph.D. Scholarship from the Ministry of Science, Research and Technology, Iran in 2004.



J. David Brown was born in Ottawa, ON, Canada, in 1977. He received the B.Sc.(Eng.) degree in electrical and computer engineering in 2000, and the M.Sc.(Eng.) degree in 2002, both from Queen's University in Kingston, ON, Canada. In 2008, he received the Ph.D. degree in electrical and computer engineering from the University of Toronto in Toronto, ON, Canada.

From 2002 to 2004 and again from 2007 to 2009, he worked as an Electrical Engineer at General Motors. In 2009, he joined the Network Information Operations Section at DRDC in Ottawa, ON, Canada, as a Research Scientist. His research interests include digital communications, error-control codes, and machine learning.

Dr. Brown has received numerous awards and scholarships, including the Natural Sciences and Engineering Research Council of Canada (NSERC) Post-graduate Scholarship, the NSERC Canada Graduate Scholarship (CGS), and two Industry Canada Fessenden Postgraduate Scholarships. He also received the Queen's University Professional Engineers of Ontario Gold Medal.



Konstantinos N. (Kostas) Plataniotis is a Professor with the Edward S. Rogers Sr. Department of Electrical and Computer Engineering at the University of Toronto in Toronto, Ontario, Canada, and an Adjunct Professor with the School of Computer Science at Ryerson University, Canada. He is the Director of The University of Toronto's Knowledge Media Design Institute (www.kmdi.utoronto.ca), and the Director of Research for the Identity, Privacy and Security Institute at the University of Toronto

(www.ipsi.utoronto.ca).

Prof. Plataniotis is the Editor in Chief (2009-2011) for the IEEE Signal Processing Letters and chairs the Examination Committee for the IEEE Certified Biometrics Professional (CBP) Program (www.ieeebiometricscertification.org). He served on the IEEE Educational Activities Board (EAB) and he was the Chair (2008-09) of the IEEE EAB Continuing Professional Education Committee. Dr. Plataniotis has served as Chair (2000-2002) IEEE Toronto Signal Processing Chapter, Chair (2004-2005) IEEE Toronto Section, and he was a member of the 2006 and 2007 IEEE Admissions & Advancement Committees.

He is the 2005 recipient of IEEE Canada's Outstanding Engineering Educator Award "for contributions to engineering education and inspirational guidance of graduate students" and the co-recipient of the 2006 IEEE Trans. on Neural Networks Outstanding Paper Award for the published in 2003 paper entitled "Face Recognition Using Kernel Direct Discriminant Analysis Algorithms".

He is a registered professional engineer in the province of Ontario, and a member of the Technical Chamber of Greece, and a Fellow of the Engineering Institute of Canada.

His research interests include biometrics, communications systems, multimedia systems, and signal & image processing.



Subbarayan Pasupathy was born in Chennai (Madras), Tamilnadu, India. He received the B.E. degree in telecommunications from the University of Madras, the M.Tech. degree in electrical engineering from the Indian Institute of Technology, Madras, and the M.Phil. and Ph.D. degree in engineering and applied science from Yale University.

Currently, he is a Professor Emeritus in the Department of Electrical and Computer Engineering at the University of Toronto, where he has been a Faculty member from 1972. His research over the

last three decades has mainly been in statistical communication theory and signal processing and their applications to digital communications. He has served as the Chairman of the Communications Group and as the Associate Chairman of the Department of Electrical Engineering at the University of Toronto. He is a registered Professional Engineer in the province of Ontario. During 1982-1989 he was an Editor for *Data Communications and Modulation* for the IEEE TRANSACTIONS ON COMMUNICATIONS. He has also served as a Technical Associate Editor for the IEEE COMMUNICATIONS MAGAZINE (1979-1982) and as an Associate Editor for the *Canadian Electrical Engineering Journal* (1980-1983). He wrote a regular humour column entitled "Light Traffic" for the IEEE COMMUNICATIONS MAGAZINE during 1984-98.

Dr. S. Pasupathy was elected as a Fellow of the IEEE in 1991 "for contributions to bandwidth efficient coding and modulation schemes in digital communication", was awarded the Canadian Award in Telecommunications in 2003 by the *Canadian Society of Information Theory*, was elected as a Fellow of the *Engineering Institute of Canada* in 2004 and as a Fellow of the *Canadian Academy of Engineering* in 2007. He was honoured as a Distinguished Alumnus by I.I.T, Madras, India in 2010. He has been identified as a "highly cited researcher" by ISI Web of Knowledge and his name is listed in ISI Highly Cited.com.